applied optics

Binary coded identification of industrial chemical vapors with an optofluidic nose

Abubakar Isa Adamu,[1,2] Fahri Emre Ozturk,[1,2] and Mehmet Bayindir[1,2,3,*]

[1]UNAM-National Nanotechnology Research Center, Bilkent University, 06800 Ankara, Turkey
[2]Institute of Materials Science and Nanotechnology, Bilkent University, 06800 Ankara, Turkey
[3]Department of Physics, Bilkent University, 06800 Ankara, Turkey
*Corresponding author: mb@4unano.com

Received 8 August 2016; revised 7 November 2016; accepted 15 November 2016; posted 16 November 2016 (Doc. ID 273337); published 13 December 2016

An artificial nose system for the recognition and classification of gas-phase analytes and its application in identifying common industrial gases is reported. The sensing mechanism of the device comprises the measurement of infrared absorption of volatile analytes inside the hollow cores of optofluidic Bragg fibers. An array of six fibers is used, where each fiber targets a different region of the mid-infrared in the range of 2–14 μm with transmission bandwidths of about 1–3 μm. The quenching in the transmission of each fiber due to the presence of analyte molecules in the hollow core is measured separately and the cross response of the array allows the identification of virtually any volatile organic compound (VOC). The device was used for the identification of seven industrial VOC vapors with high selectivity using a standard blackbody source and an infrared detector. The array response is registered as a unique six digit binary code for each analyte by assigning a threshold value to the fiber transmissions. The developed prototype is a comprehensive and versatile artificial nose that is applicable to a wide range of analytes.

OCIS codes: (250.3750) Optical logic devices; (160.5293) Photonic bandgap materials; (300.6340) Spectroscopy, infrared; (350.2450) Filters, absorption.

https://doi.org/10.1364/AO.55.010247

1. INTRODUCTION

Gas-phase chemical sensing has been an active field for decades and has expanded exponentially with new scientific advancements, such as the introduction of nanotechnology [1–4]. A great variety of applications, ranging from toxic chemical detection to disease diagnostics has been investigated [5–7] and these studies have found practical uses on an individual consumer level, such as fire or natural gas alarms. However, there are challenges in the commercialization of gas sensors for applications where identification of multiple chemicals is required, such as food and water safety and environmental monitoring [8,9]. For instance, for indoor air quality monitoring, the target molecules are an enormous range of volatile organic compounds (VOCs) that evaporate from products such as paint, varnishes, cleaning supplies, pesticides, and furnishings [9,10]. An analytical tool that can be used for such purposes should be able to accurately recognize a wide range of VOCs while addressing the challenges of complexity, size, and cost of conventional systems.

A promising solution to successfully distinguish multiple analytes is to use an array of sensors, each responsive to several different analytes, in contrast with the conventional "lock-and-key" sensors, which are specific to a single analyte [11]. Sensor arrays are also called artificial noses [12–15] as their development was inspired by the mammalian nose, where the cross response of various types of sensory proteins, each responsive to a number of different chemicals, are registered to distinguish odors [16]. This approach enables the nose to classify and recognize several different analytes by the unique response of the sensor array to each of them [11]. Artificial noses employing arrays of a great variety of sensor technologies have been used for the successful detection and identification of gaseous species [15]. The difficulty in the development of a simple, practical, and cost-effective artificial nose arises due to the limitations of the employed sensor technologies. For instance, transduction mechanisms that directly measure the physical properties, such as the change in resistance [17–19] or refractive index [20–22], are too non-specific for the recognition of analytes. This leads to the use of highly complex recognition setups [23] or signal interpretation methods [24–26] coupled with the sensor to achieve a reliable selectivity. Alternatively, the surface of the transducers is functionalized with chemical [27–30] or biological [31–33] recognition layers. To ensure the desired selectivity, each transducer in the array

needs to be specific to a different set of analytes than the other. This requires the immobilization of different biological receptor types or employment of different reactive chemicals to each transducer, which substantially increases the complexity and cost of the system. These problems are usually intertwined with others, such as the impractical response times, temperature dependence and limited reusability, which hinders the development of an all-around artificial nose.

A competent alternative to artificial noses that could address these problems is the measurement of the light absorption of analyte gases in hollow waveguides [34,35] or gas cells [5]. Mid-infrared absorption is particularly promising for the detection and identification of chemicals as most chemicals have specific absorption bands within this range and the electromagnetic wave absorption is several times higher compared to shorter wavelengths [5,36]. Discerning target molecules by their absorption bands requires the coverage of a wide wavelength range with good spectral resolution in the measurements. Additionally, long optical path lengths are necessary to ensure the desired sensitivity, as stated by the Beer–Lambert law. Several techniques were developed to overcome the issues of optical path length and wavelength selectivity. These methods incorporate a monochromator or interferometer system [37,38,39], tunable monochromatic light sources [40,41], or wavelength filters [42] to determine the absorption wavelengths. The wavelength selective parts are coupled with different optical cavity designs or waveguides to enhance the light–analyte interaction [5,36,37,38]. However, the size reduction of these systems remained limited as the solution of this two-sided problem requires a straightforward approach that can address the issues of wavelength selectivity and long optical path lengths simultaneously.

In our previous studies, we showed an optofluidic nose concept that combines the sensor array approach of artificial noses and the advantages of light absorption-based methods in the mid-infrared [43]. This is achieved with the cross response of an array of hollow-core Bragg fibers [44,45], i.e., wavelength-scalable infrared photonic bandgap fibers. Bragg fibers have dielectric mirrors (high refractive index contrast multilayered structures) surrounding their hollow cores and therefore their transmission is at a specific band of the electromagnetic spectrum. The spectral location and bandwidth of the photonic bandgap can be tuned during the fiber drawing in the whole mid-infrared range [45,46]. In this optofluidic nose concept, the array of Bragg fibers, each transmitting at a different band in the mid-infrared, functions as an infrared filter array and hollow waveguides simultaneously to ensure long path lengths and wavelength selectivity. The cross response of the array is a unique signature of the analyte's infrared absorption and allows the selective identification of virtually any target molecule [47,48].

In this work, we developed an artificial nose system for the recognition and classification of gas-phase analytes and tested its application in identifying common industrial gases. We report the first prototype of the optofluidic nose and use it for the identification of seven common industrial VOC vapors. At the core of the device is an array of six Bragg fibers that scan the mid-infrared region of 2–14 μm. The device used a simple blackbody source, an HgCdTe (MCT) infrared detector coupled to the fiber array, and additional simple, low-cost optical and electrical elements. Each chemical can be tagged with a unique binary code by addressing the fibers separately and by assigning a threshold value to each, allowing a simple data analysis. An excellent selectivity that recognized the tested VOC vapors in repeated measurements and classified them with unique six-digit binary codes was demonstrated.

2. EXPERIMENTAL METHODS

A. Selection of Fibers Transmissions

The multilayer thickness ($t_{(a,b)}$) of the Bragg fibers are calculated by $t_{(a,b)} = \lambda/4n_{(a,b)}$, where n_a and n_b stand for the refractive indices of chalcogenide and polymer, respectively, while $t_{(a)}$ and $t_{(b)}$ stand for their individual thicknesses. The omnidirectional band or photonic bandgap center, λ, is targeted to match the analyte's absorption spectrum within the fingerprint region.

B. Fabrication of the Bragg Fiber Array

Hollow-core infrared Bragg fibers were prepared by thermal drawing in a custom-made fiber tower. Details of the fiber fabrication process were previously reported [45,48,46]. The fabrication process consists of three main steps: the preparation of polymer and chalcogenide through thermal evaporation, followed by the winding and consolidation of the preform and finally the drawing of the preform from a fiber tower. In the first step, pieces of chalcogenide glass (As_2Se_3) are ground to fine sizes with a mechanical grinder, then using thermal evaporation, the arsenic selenide is grown on the polyethersulfone (PES) polymer film of thickness 50 μm. To improve the deposition growth process, the polymer film first undergoes plasma treatment to activate the surface and enhance surface reaction during deposition. After a thin layer of chalcogenide is grown on both sides of the polymer film, the preform was prepared by rolling the layers of coated polymer around a glass rod of 18 cm in diameter. The ratio of the chalcogenide coating (refractive index of about 2.8) and polymer film (refractive index of about 1.6) thicknesses were arranged to form high refractive index contrast quarter-wave stack multilayers as the coated films are rolled into a cylinder. The next step is the consolidation of the preform in vacuum at 180°C for 4 h, then heat further to 255°C for 35 min. The end product after this is a solid composite rod with glass in the middle. The glass is then etched out with hydrofluoric acid. The final step is the fiber drawing: the obtained polymer/chalcogenide composite rod (preform) is fed to the furnace of a fiber tower and drawn under controlled load and temperature [Fig. 1(a)]. Through the thermal drawing of the fiber, the quarter-wave stack period of the preform is scaled down by a controllable factor. The furnace is gradually heated to 298°C, which is above the glass transition temperature of both PES and As_2Se_3. An adjustable load is applied from the bottom of the preform simultaneously. The preform starts to form a neck and elongate from the bottom, and the elongated preform forms the hollow-core Bragg fibers. The fabricated fiber is collected at various desired lengths and scanned for their transmission. The array of six hollow-core fibers used in this study is shown in Fig. 1(b). The fibers have lengths of approximately 30 cm, diameters of about 1–2 mm,

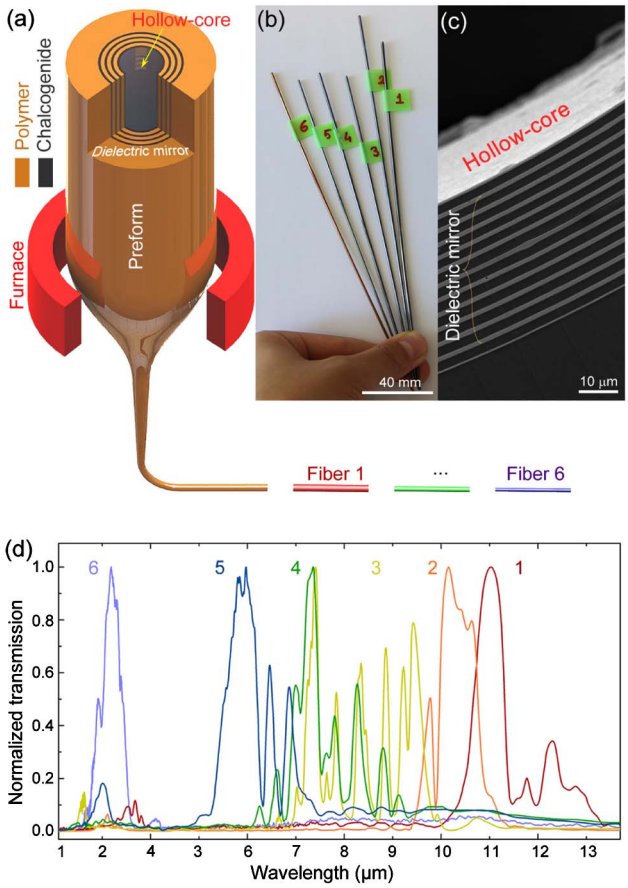

Fig. 1. Wavelength scalable hollow-core Bragg fibers with photonic bandgaps at different parts of the mid-infrared wavelengths. (a) Thermal fiber drawing allows scaling down the diameter, and the quarter-wave stack period of the dielectric mirrors (polymer/chalcogenide multilayers) along with it simultaneously. This allows tuning the bandgap of the fiber during the drawing. (b) The array of Bragg fibers used in this study. (c) The SEM image of Fiber 1, showing the multilayer stack (dielectric mirror) and hollow core where volatile chemical molecules are introduced and the infrared light is coupled to the fiber simultaneously to measure the change in transmission with the presence of the analyte. (d) The transmission spectra of the six fabricated fibers, which covers the fingerprint region.

and hollow-core diameters ranging from 300 to 800 μm. The photonic bandgaps of the fibers can be adjusted during the drawing by controlling the fiber diameter. Figure 1(c) shows the cross section of Fiber 1 with 13 bilayers of As_2Se_3 and PES, which forms the multilayered dielectric mirror structure centered around 11 μm wavelength. The six-fiber array is designed to scan the wavelength range of 2–14 μm and target different absorption bands of the chemicals. The transmission spectra of the fibers were measured by taking transmission measurements with a Fourier transform infrared spectrometer (FTIR–Bruker, Tensor 37) and are shown in Fig. 1(d). Each fiber has a photonic bandgap centered at a different spectral position of the mid-infrared. It is seen from Fig. 1(d) that the transmission spectra of some fibers do not have single peak (e.g., Fiber 3 has several peaks around 8 μm) due to the fact that the PES polymer has absorption bands at the mid-infrared range, and this interferes with the transmission profile of the fiber. To circumvent this problem, an all-chalcogenide multilayer fiber can be used, since chalcogenides have no absorption at these wavelength ranges [49]. Furthermore, a sharper peak can be attained by tapering the fiber during thermal drawing; these conical fibers have been shown to eliminate higher-order transmission bands and also narrow the fundamental band [46]. For the determination of fiber transmission bands, the blackbody light from the FTIR source was coupled to the Bragg fibers and the transmittance was measured by aligning the fiber end to the externally used detector of the FTIR. The FTIR was used for specifying the transmission bands, and not for the analyte quenching measurements.

C. Optofluidic Nose Setup

Figure 2(a) shows the experimental setup of the optofluidic nose system and the photograph of the setup is given in Fig. 2(b). The method relies on taking the cross response of the six fibers in the array to recognize the chemical vapors.

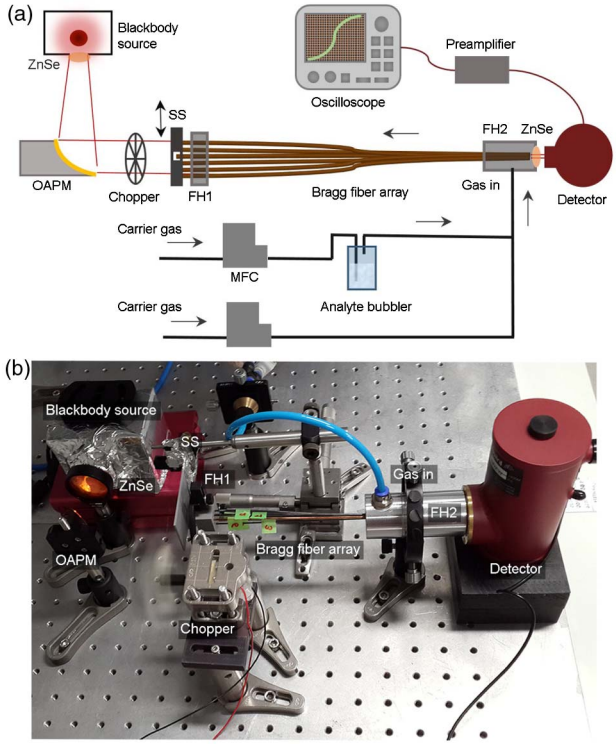

Fig. 2. (a),(b) The optofluidic nose measurement setup. OAPM, off-axis parabolic gold mirror; SS, shutter stage; FH, fiber holder; ZnSe, zinc selenide infrared lens; MCT, mercury cadmium telluride infrared detector; MFC, mass flow controller. FH1 is used to hold the tips of the fibers at equal intervals. Industrial chemical vapors are introduced to the fiber array through FH2, which is sealed against leaks and which allows the coupling of the infrared light to the MCT detector. A manual shutter stage is used to couple the broadband infrared light to a single fiber at a time, to allow addressing each fiber separately. The light from the blackbody source (silicon nitride heating element) is aligned to a beam with the ZnSe lens and OAPM. An electric motor is implemented as a chopper for the modulation of light. A commercial preamplifier circuit and an oscilloscope is used for the signal readout. Nitrogen carrier gas is saturated with the analyte vapor in the analyte bubbler with the constant flow of the MFC.

The response of each fiber is the quenching in its transmitted intensity due to the infrared absorption of analyte molecules at the hollow fiber cores. Accordingly, the measurements comprise the measurement of the transmitted intensity of each fiber before and after analyte introduction. The developed optofluidic nose device employed a single blackbody source [silicon nitride heating element from Crystal-Technica (UK)] to ensure a broadband emission covering the whole 2–12 μm range. The light from the blackbody source was collimated to a beam of a few centimeters diameter with an off-axis parabolic gold mirror. The tips of the fibers were aligned to the beam. An electric motor was employed as a chopper to modulate the radiation for the HgCdTe (MCT) infrared detector [InfraRed Associates Inc., MCT-13-2.00 (MSL-8)]. A shutter stage was employed at the fiber tips to allow the coupling of the broadband radiation to only a single fiber at a time, and by moving the shutter slit to the fiber end the transmission of each fiber was measured separately. The fibers were aligned with equal intervals with a custom design 3D printed fiber holder (FH1). A second fiber holder (FH2) was employed for the introduction of analyte gas into the fibers and for the coupling of the transmitted light to the MCT. FH2 allows the flow of analyte vapor and carrier gas through the hollow core of the fiber, and the coupling of the broadband IR light to the fiber simultaneously. It comprises aluminum parts that are sealed against gas leakage and a ZnSe infrared lens at one end. The ZnSe end is aligned with the MCT to allow maximum coupling of the transmitted light from the ends of the fibers to the MCT. The MCT is operated with a commercial preamplifier (Infrared Systems Development, MCT-1000 Current Mode Preamplifier) and the detector response is read out with an oscilloscope (LeCroy, WaveAce 112). For the analyte introduction, two mass flow controllers (MKS, multi gas controller 647) were connected in parallel, to provide a controlled gas flow into fiber cores. The mass flow controllers (MFCs) were attached to a nitrogen gas canister, for the supply of nitrogen as the carrier gas. The analyte vapors at room temperature were taken from bubblers with one of the MFCs and flowed through the hollow cores of all fibers in the array simultaneously. Nitrogen was saturated with the analyte vapors at the analyte bubblers under constant flow, which was adjusted by the MFC. The second MFC was used to purge the fiber cores before and after each analyte measurement.

D. Measurements and Data Analysis

All measurements were taken at room temperature (varying between 15°C and 22°C) and under ambient humidity. For the measurements, the background signal of each fiber in the array (the transmitted intensity of the fiber without the presence of analyte molecules in the hollow core) was taken after the fiber cores were purged with carrier nitrogen gas. The shutter stage was employed for rapidly taking the background measurements of each fiber, without any other adjustments in the setup. After the background measurements, the analyte gas was flowed through the fiber array and the measurements were repeated with the presence of analyte molecules in the hollow cores of the fibers. The MCT readout for each of the fibers was recorded in electrical potential units from the oscilloscope. Three measurements were taken for each analyte–fiber combination. The detector readout was converted to the fiber response by $[(S - S_0)/S_0) * 100]$, where S_0 is the background signal read from the MCT before the analyte introduction and S is the signal after the analyte introduction. The averages and standard deviations of the fiber responses were used to determine threshold values of each fiber to register the response of the fiber in binary logic. The threshold values were selected considering the reliability of the recognition in repeated measurements. For this purpose, threshold values that ensure a unique binary code to each analyte were chosen outside the standard deviation in the fiber responses. Accordingly, the threshold is determined after the responses of the whole array have been calculated, by considering which chemicals each fiber can differentiate with the selected threshold value. For example, since benzene and toluene are chemically similar species, the responses of the fibers are similar for these analytes. Therefore, care is taken when determining the threshold of 25% for Fiber 6 to ensure that the fiber can distinguish these two chemicals in binary codes. The fiber responses to each of the seven tested chemical vapors and the corresponding binary codes were converted to color scale with a commercial software. The table of responses for each fiber to the seven chemicals is presented in the supplementary document as well as their corresponding binary codes.

It should be stressed that the use of binary coding is not practical with varying concentrations of analytes. The main reason for this limitation is the infinite number of binary code combinations that would be needed if the concentration is included as a varying factor. An array of six fibers allows 64 different combinations and it is not possible to address each analyte concentration with a unique binary code. For studies where the concentration determination is required or when working with mixtures of different analytes with varying volume ratios, it is more convenient to use pattern recognition techniques such as hierarchical cluster analysis or principal component analysis [48]. For instance, if the concentration of acetone is increased above 2000 ppm, the response of Fiber 2 will increase above 35% and the fiber will tag acetone with a "1" instead of a "0." This will mean that Fiber 2 will tag acetone the same way with ethyl acetate. Therefore varying the concentration would raise the need for additional digits that would separate high concentrations of acetone with lower concentrations. The response of the Fiber 2 to acetone at varying temperatures and concentrations. For these reasons, we have kept the analyte concentrations constant during the measurements.

Acetic acid and ethyl acetate were purchased from Sigma-Aldrich, acetone from Carlo Erba, benzene and formaldehyde from Panreac, hexane from Emplura, and toluene from Emsure. All chemicals were used as received.

3. RESULTS AND DISCUSSION

A. Fiber Response to Chemical Vapors

Six hollow-core Bragg fibers with transmission bandwidths ranging from 1 to 3 μm at different spectral positions in the mid-infrared were employed for the optofluidic nose. The photonic bandgaps (transmission bands) of the fibers were arranged to scan the range of 2–14 μm, where most chemicals have specific absorption bands. The transmission spectra of the six fibers are shown in Fig. 1(b). The photonic bandgap of Fiber 1 is

centered at 12 μm, Fiber 2 at 10.5 μm, Fiber 3 at 8.5 μm, Fiber 4 at 7.5 μm, Fiber 5 at 6 μm, and Fiber 6 at 3.3 μm. Most chemicals have several narrow and dense absorption peaks (often narrower than the transmission bandwidth of the fiber) in the 2–14 μm range, as it is related to the vibrational and rotational modes of molecules. The responses of the fibers are the percentage of quenching in their transmitted intensity when the analytes are introduced to the hollow fiber cores. The transmission band of a single fiber is often overlapping with the absorption bands of several different analytes, which results in a quenching of fiber transmission when these analytes are introduced to the fiber core. Therefore, each fiber in the array is not specific to a single, but to several different analytes. The magnitude of the response of the fiber is directly related with the extent of overlap between the absorption bands of the analyte and transmission band of the fiber. This results in a selective response to multiple analytes, i.e., each fiber responds to the analytes at varying degrees. For instance, Figs. 3(a) and 3(b) show the response of Fiber 2 to toluene and ethyl acetate vapors. Since the only overlapping of the transmission band of Fiber 2 (centered at 10.5 μm) is with the sideband of the absorption band of toluene centered at 9.5 μm, there is only a slight (4%) quenching of Fiber 2 transmission [Fig. 3(a)]. In comparison, two ethyl acetate absorption bands, centered at 9 and 11 μm, are overlapping with the transmission of Fiber 2 [Fig. 3(b)]. Accordingly, the response of Fiber 2 to ethyl acetate is about 45%. The responses of Fiber 2 to all seven chemical vapors tested in this study are shown in Fig. 3(c). Three separate measurements were taken with each analyte to calculate average and standard deviation of the fiber responses. As can be expected with a mid-infrared sensor, even a single fiber is very selective, with significant difference in the responses to most of the analytes. In the case of Fiber 2, the response is not specific enough to distinguish between acetic acid–ethyl acetate and formaldehyde–benzene. This does not hinder the performance of the device, however, as with artificial noses the purpose of each sensing element in the array is not to determine a specific analyte but to supply a broad and versatile response.

The selectivity of the fiber response and the versatility to respond to multiple analytes is exploited for simple classification and recognition of analytes. As each fiber is addressed separately during the measurements, it is possible to assign a threshold value to each fiber and register the response as a true (1) or false (0) in Boolean algebra. In this approach, if the fiber response is higher than a predetermined threshold value, the chemical is tagged with a "1" for the measurement with this particular fiber. If the response is lower than the threshold it is tagged as "0." The response of the six-fiber array then can be obtained as a six-digit binary code for each chemical vapor. Figure 3(d) shows the response of Fiber 2 to each of the chemical vapors in color code. A threshold value of 35% was determined for Fiber 2, which tagged acetic acid and ethyl acetate as "1" and the remaining chemical vapors (hexane, formaldehyde, acetone, benzene, and toluene) as "0" [Fig. 3(d)]. As there are

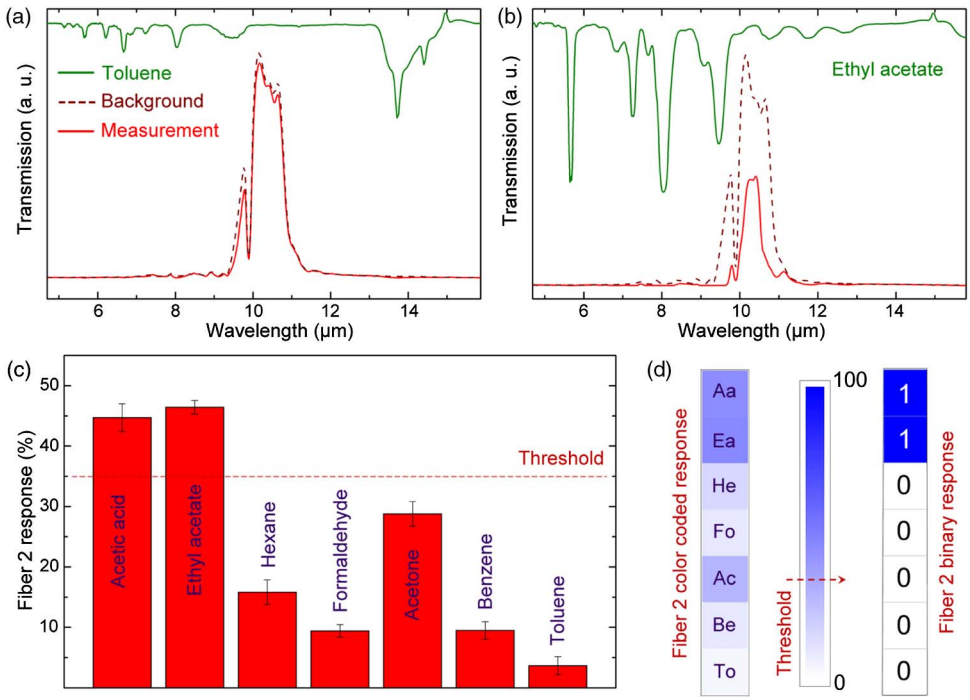

Fig. 3. Response of Fiber 2 to industrial chemical vapors. (a) There is no significant overlap of the transmission band of Fiber 2 and the absorption bands of toluene vapor, resulting in only a slight quenching (4%) in transmission with the presence of toluene molecules in the fiber core. (b) The transmission of the Fiber 2 is quenched 45% from the initial value in ethyl acetate measurement due to the absorption bands at 9 and 11 μm. (c) The response of Fiber 2 to the seven different common industrial chemical vapors. (d) Binary coded representation of Fiber 2 response. Blue scale representation of the Fiber 2 response to the chemicals. The determined threshold value of 35% tags acetic acid and ethyl acetate with a "1" whereas the remaining chemical vapors are tagged with a "0." (Aa, acetic acid; Ea, ethyl acetate; He, hexane; Fo, formaldehyde; Ac, acetone; Be, benzene; To, toluene).

only two possible codes in binary logic, a "1" and a "0," the binary coding of the response of a single fiber is not useful for identifying the analytes. However, the possible codes that the analytes can be tagged with increases exponentially with the total number of possible tags being 2[n], where n is the total number of fibers.

B. Recognition and Classification of Industrial Chemical Vapors

When applied to each of the fibers in the array, the binary coding approach allows simple classification and recognition of analytes without the need of employing any pattern recognition techniques, such as hierarchical cluster analysis or principal component analysis. The responses of each fiber in the six-fiber array to the chemical vapors were measured by introducing the chemical vapor to the hollow cores of the fibers in the array simultaneously and rapidly measuring the quenching in each fiber's transmission. The transmitted intensity of the fibers was recorded before and after analyte introduction to the array. The scheme of the measurement setup is shown in Fig. 2. The response time of the fibers is very fast (subsecond) as it is only limited with the response time of the infrared detector and not with the adsorption of the analyte to any recognition layer. Additionally, the signal recovers completely after the fibers are purged with the carrier gases; no analyte residue remains in the hollow fiber cores. The response of each fiber was calculated by comparing the quenching in the fiber transmission with analyte introduction, as explained in the example of Fiber 2 in the previous section. The color-coded average responses of the array to all seven tested industrial chemical vapors are shown in Fig. 4(a). A unique set of responses to each of the industrial chemical vapors is demonstrated with the developed straightforward optofluidic nose system demonstrating the robust selectivity. It should be noted that there is potential for further miniaturization of this device for the development of portable mid-infrared optofluidic noses. The mass flow controllers can be replaced with a simple fan, and the oscilloscope with a readout circuit in a portable design. The MCT, which is the most expensive element in the device, can be replaced with more compact and low-cost broadband infrared detectors, such as pyroelectric deuterated, L-alanine doped triglycine sulfate (DLATGS) detectors. Using the full potential of mid-infrared hollow waveguide sensing techniques and the sensor array approach of the artificial noses reduces the need for expensive instrumentation and design complexity.

To register the fiber response data as a binary code, a separate threshold value was determined for each fiber. Since the responses of the fibers vary greatly from analyte to analyte, there is a significant flexibility during the determination of threshold values. Proper threshold values that will produce a unique binary code to each chemical vapor in repeated measurements were determined considering the standard deviations of each of the measurements. Once the threshold values have been determined for each of the six fibers in the array and each chemical is tagged with a unique six-digit binary code, there is no need to make any further adjustments for a repeatable and reliable recognition. The threshold values were determined as 10% for Fiber 1, 35% for Fiber 2, 30% for Fiber 3, 7% for Fiber 4, 20% for Fiber 5, and 25% for Fiber 6 and are shown in color code in Fig. 4(a). The binary codes of the tested chemicals as registered by the optofluidic nose with these thresholds are shown in Fig. 4(b). Each chemical vapor was classified with a unique binary code. It should be noted that the transmission bands of different fibers in the array often overlap [Fig. 1(d)]. In artificial nose systems, each sensing element is intended to respond to a large number of analytes, rather than being analyte specific. The cross response of broadly responsive sensing elements yields a high selectivity. For instance, Fiber 3 and Fiber 4, which have the broadest overlapping transmission bands, respond differently to most of the analytes [Fig. 4(a)]. The binary codes read from these fibers after applying the threshold values are different for acetic acid, hexane, benzene, and toluene [Fig. 4(b)].

It is interesting to note that chemicals with similar molecular structures have similar binary codes with the optofluidic nose. For instance, acetic acid and ethyl acetate differ only in their functional groups bonded to the oxygen atom in the carboxylic acid. Accordingly, acetic acid is tagged with "110111" with the

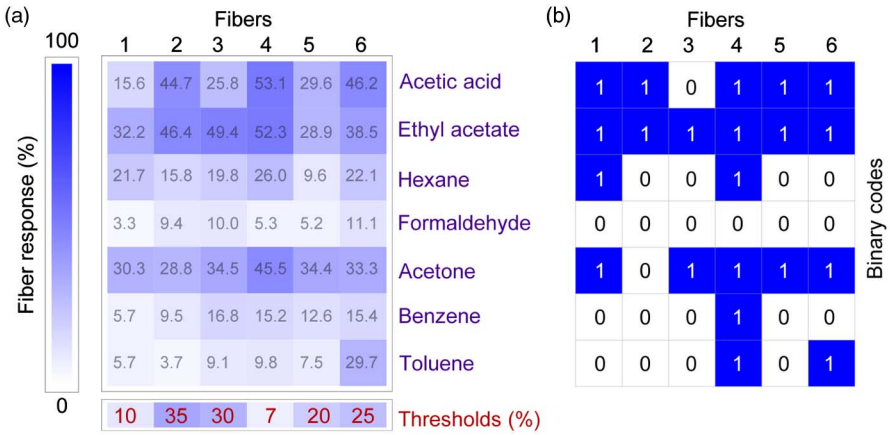

Fig. 4. Binary coded identification of the industrial chemical vapors with the fiber array. (a) Color code representation of the six-fiber array response. Even chemically similar species such as benzene and toluene are recognized with a unique set of fiber responses. The determined threshold values for each of the fibers are shown in color code. (b) The binary coded array response with the determined threshold values is shown for each of the seven chemicals. Each chemical is identified with a unique six-digit code.

optofluidic nose, whereas the binary codes of ethyl acetate differ only in the third fiber with "111111." Similarly, toluene "000101" is distinguished from benzene "000100" only with the methyl group ($-CH_3$) attached to a phenyl group ($-C_6H_5$). This effective classification is a benefit of directly measuring the mid-infrared absorption of molecules. The spectral location and strength of the absorption bands of chemically similar species are alike as the infrared absorption bands are originated from molecular bonds and vibrational or rotational modes of molecules. With the developed optofluidic nose, the seven tested common industrial chemical vapors were accurately cataloged and classified simply with digital codes.

4. CONCLUSIONS

The optofluidic nose identified a wide range of industrial chemical vapors with six-digit binary codes. The developed system is a combination of hollow waveguide mid-infrared sensor technologies with artificial noses. This is made available by the unique features of Bragg fibers that can be employed as infrared photonic bandgap filters, waveguides, and gas cells simultaneously. The spectral positions of the photonic bandgap of each Bragg fiber in the array of six was chosen to address different absorption bands of chemicals in the mid-infrared region. This allows the use of a standard blackbody source and infrared detector coupled to the fiber array to demonstrate a competitive selectivity that is quite challenging to achieve in conventional methods. The results reported here demonstrate a straightforward approach that completely eliminates the need for both surface functionalized recognition layers in the conventional artificial noses and expensive wavelength tunable lasers or bulky monochromators in miniaturized infrared sensor technologies, which have comparable selectivity to the developed device. The response of the fiber array was registered as a unique binary code for each chemical vapor by applying a threshold value to the responses of each fiber. This simplified the data analysis, eliminating the need for employing any pattern recognition and enabled cataloging of the chemicals simply with digital codes. It should be stressed that the developed system is not limited to the identification of industrial chemical vapors. Due to the direct association of the absorption bands in the mid-infrared region with the molecular structures, virtually any gas can be detected with this method. The developed system has the potential to be a competent alternative to emerging technologies in both highly selective artificial noses and quantum cascade laser-based detection systems.

Funding. TUBITAK (113T069).

Acknowledgment. We gratefully thank Adem Yildirim, Hasan Güner, Urandelger Tuvshindorj, Gokcen Birlik Demirel, Muhammad Yunusa, and Pınar Beyazkılıç for fruitful discussions. We also thank Murat Dere for his help during the drawing of fibers.

REFERENCES

1. M. Li, E. Myers, H. Tang, S. Aldridge, H. McCaig, J. Whiting, R. Simonson, N. Lewis, and M. Roukes, "Nanoelectromechanical resonator arrays for ultrafast, gas-phase chromatographic chemical analysis," Nano Lett. **10**, 3899–3903 (2010).
2. T. Kelly, A. Sega, and M. Sailor, "Identification and quantification of organic vapors by time-resolved diffusion in stacked mesoporous photonic crystals," Nano Lett. **11**, 3169–3173 (2011).
3. P. Clement, S. Korom, C. Struzzi, E. Parra, C. Bittencourt, P. Ballester, and E. Llobet, "Deep cavitand self-assembled on Au NPs-MWCNT as highly sensitive benzene sensing interface," Adv. Funct. Mater. **25**, 4011–4020 (2015).
4. F. Rock, N. Barsan, and U. Weimar, "Electronic nose: current status and future trends," Chem. Rev. **108**, 705–725 (2008).
5. J. Hodgkinson and R. P. Tatam, "Optical gas sensing: a review," Meas. Sci. Technol. **24**, 012004 (2013).
6. Y. Yamada, S. Hiyama, T. Toyooka, S. Takeuchi, K. Itabashi, T. Okubo, and H. Tabata, "Ultratrace measurement of acetone from skin using Zeolite: toward development of a wearable monitor of fat metabolism," Anal. Chem. **87**, 7588–7594 (2015).
7. Z. Yuan, F. Lu, M. Peng, C. Wang, Y. Tseng, Y. Du, N. Cai, C. Lien, H. Chang, Y. He, and E. Yeung, "Selective colorimetric detection of hydrogen sulfide based on primary amine-active ester cross-linking of gold nanoparticles," Anal. Chem. **87**, 7267–7273 (2015).
8. R. Farahi, A. Passian, L. Tetard, and T. Thundat, "Critical issues in sensor science to aid food and water safety," ACS Nano **6**, 4548–4556 (2012).
9. E. Etzov, A. Cohen, and R. Marks, "Bioluminescent liquid light guide pad biosensor for indoor air toxicity monitoring," Anal. Chem. **87**, 3655–3661 (2015).
10. United States Environmental Protection Agency, http://www.epa.gov/iaq/pubs/careforyourair.html#learn, 29 August 2015.
11. K. J. Albert, N. S. Lewis, C. L. Schauer, G. A. Sotzing, S. E. Stitzel, T. P. Vaid, and D. R. Walt, "Cross-reactive chemical sensor arrays," Chem. Rev. **100**, 2595–2626 (2000).
12. K. Persaud and G. Dodd, "Analysis of discrimination mechanisms in the mammalian olfactory system using a model nose," Nature **299**, 352–355 (1982).
13. N. A. Rakow and K. S. Suslick, "A colorimetric sensor array for odour visualization," Nature **406**, 710–713 (2000).
14. T. A. Dickinson, J. White, J. S. Kauer, and D. R. Walt, "A chemical-detecting system based on a cross-reactive optical sensor array," Nature **382**, 697–700 (1996).
15. S. E. Stitzel, M. J. Aernecke, and D. R. Walt, "Artificial noses," Annu. Rev. Biomed. Eng. **13**, 1–25 (2011).
16. L. Buck and R. Axel, "A novel multigene family may encode odorant receptors: a molecular basis for odor recognition," Cell **65**, 175–187 (1991).
17. V. Dobrokhotov, L. Oakes, D. Sowell, A. Larin, J. Hall, A. Kengne, P. Bakharev, G. Corti, T. Cantrell, T. Prakash, J. Williams, and D. McIlroy, "Toward the nanospring-based artificial olfactory system for trace-detection of flammable and explosive vapors," Sens. Actuators B **168**, 138–148 (2012).
18. V. V. Sysoev, J. Goschnick, T. Schneider, E. Strelcov, and A. Kolmakov, "A gradient microarray electronic nose based on percolating SnO_2 nanowire sensing elements," Nano Lett. **7**, 3182–3188 (2007).
19. C. Weber, M. Cauchi, M. Patel, C. Bessant, C. Turner, L. Britton, and C. Willis, "Evaluation of a gas sensor array and pattern recognition for the identification of bladder cancer from urine headspace," Analyst **136**, 359–364 (2011).
20. S. Choi, M. Mamak, G. von Freymann, N. Chopra, and G. Ozin, "Mesoporous Bragg stack color tunable sensors," Nano Lett. **6**, 2456–2461 (2006).
21. J. Kobler, B. Lotsch, G. Ozin, and T. Bein, "Vapor-sensitive Bragg mirrors and optical isotherms from mesoporous nanoparticle suspensions," ACS Nano **3**, 1669–1676 (2009).
22. T. Jalkanen, V. Torres-Costa, J. Salonen, M. Bjorkqvist, E. Makila, J. Martinez-Duart, and V. Lehto, "Optical gas sensing properties of thermally hydrocarbonized porous silicon Bragg reflectors," Opt. Express **17**, 5446–5456 (2009).
23. I. Chae, D. Lee, S. Kim, and T. Thundat, "Electronic nose for recognition of volatile vapor mixtures using a nanopore-enhanced opto-calorimetric spectroscopy," Anal. Chem. **87**, 7125–7132 (2015).

24. L. D. Bonifacio, G. A. Ozin, and A. C. Arsenault, "Photonic nose-sensor platform for water and food quality control," Small **7**, 3153–3157 (2011).
25. A. Ozmen, F. Tekce, M. Ebeoglu, C. Tasaltin, and Z. Ozturk, "Finding the composition of gas mixtures by a phthalocyanine-coated QCM sensor array and an artificial neural network," Sens. Actuators B **115**, 450–454 (2006).
26. N. Speller, N. Siraj, B. Regmi, H. Marzoughi, C. Neal, and I. Warner, "Rational design of QCM-D virtual sensor arrays based on film thickness, viscoelasticity, and harmonics for vapor discrimination," Anal. Chem. **87**, 5156–5166 (2015).
27. J. Askim, M. Mahmoudi, and K. Suslick, "Optical sensor arrays for chemical sensing: the optoelectronic nose," Chem. Soc. Rev. **42**, 8649–8682 (2013).
28. S. H. Lim, L. Feng, J. W. Kemling, C. J. Musto, and K. S. Suslick, "An optoelectronic nose for the detection of toxic gases," Nat. Chem. **1**, 562–567 (2009).
29. H. Xu, K. Cao, H. Ding, Q. Zhong, H. Gu, Z. Xie, Y. Zhao, and Z. Gu, "Spherical porphyrin sensor array based on encoded colloidal crystal beads for VOC vapor detection," ACS Appl. Mater. Interfaces **4**, 6752–6757 (2012).
30. S. Harbeck, D. Atilla, I. Dulger, M. Harbeck, A. Gurek, Z. Ozturk, and V. Ahsen, "The role of hydrogen bonding in the sensitivity of QCM sensors: a spectroscopic study on tosylamido phthalocyanines," Sens. Actuators B **191**, 750–756 (2014).
31. H. Pei, J. Li, M. Lv, J. Wang, J. Gao, J. Lu, Y. Li, Q. Huang, J. Hu, and C. Fan, "A graphene-based sensor array for high-precision and adaptive target identification with ensemble aptamers," J. Am. Chem. Soc. **134**, 13843–13849 (2012).
32. J. Liu, G. Li, X. Yang, K. Wang, L. Li, W. Liu, X. Shi, and Y. Guo, "Exciton energy transfer-based quantum dot fluorescence sensing array: chemical noses for discrimination of different nucleobases," Anal. Chem. **87**, 876–883 (2015).
33. S. Qian and H. Lin, "Colorimetric sensor array for detection and identification of organophosphorus and carbamate pesticides," Anal. Chem. **87**, 5395–5400 (2015).
34. J. Harrington, "A review of IR transmitting, hollow waveguides," Fiber Integr. Opt. **19**, 211–227 (2000).
35. J. Rohwedder, C. Pasquini, P. Fortes, I. Raimundo, A. Wilk, and B. Mizaikoff, "iHWG-μNIR: a miniaturised near-infrared gas sensor based on substrate-integrated hollow waveguides coupled to a micro-NIR-spectrophotometer," Analyst **139**, 3572–3576 (2014).
36. S. Kim, C. Young, and B. Mizaikoff, "Miniaturized mid-infrared sensor technologies," Anal. Bioanal. Chem. **390**, 231–237 (2008).
37. C. Young, N. Menegazzo, A. Riley, C. Brons, F. DiSanzo, J. Givens, J. Martin, M. Disko, and B. Mizaikoff, "Infrared hollow waveguide sensors for simultaneous gas phase detection of benzene, toluene, and xylenes in field environments," Anal. Chem. **83**, 6141–6147 (2011).
38. J. Yang, J. Her, and S. Chen, "Development of an infrared hollow waveguide as a sensing device for detection of organic compounds in aqueous solutions," Anal. Chem. **71**, 3740–3746 (1999).
39. J. Petruci, P. Fortes, V. Kokoric, A. Wilk, I. Raimundo, A. Cardoso, and B. Mizaikoff, "Real-time monitoring of ozone in air using substrate-integrated hollow waveguide mid-infrared sensors," Sci. Rep. **3**, 198–203 (2013).
40. K. Worle, F. Seichter, A. Wilk, C. Armacost, T. Day, M. Godejohann, U. Wachter, J. Vogt, P. Radermacher, and B. Mizaikoff, "Breath analysis with broadly tunable quantum cascade lasers," Anal. Chem. **85**, 2697–2702 (2013).
41. J. van Helden, N. Lang, U. Macherius, H. Zimmermann, and J. Ropcke, "Sensitive trace gas detection with cavity enhanced absorption spectroscopy using a continuous wave external-cavity quantum cascade laser," Appl. Phys. Lett. **103**, 131114 (2013).
42. M. Calderisi, A. Ulrici, S. Sinisalo, J. Uotila, and R. Seeber, "Simulation of an experimental database of infrared spectra of complex gaseous mixtures for detecting specific substances. The case of drug precursors," Sens. Actuators B **193**, 806–814 (2014).
43. A. Yildirim, M. Vural, M. Yaman, and M. Bayindir, "Bioinspired optoelectronic nose with nanostructured wavelength-scalable hollow-core infrared fibers," Adv. Mater. **23**, 1263–1267 (2011).
44. P. Yeh, A. Yariv, and E. Marom, "Theory of Bragg fiber," J. Opt. Soc. Am. **68**, 1196–1201 (1978).
45. B. Temelkuran, S. D. Hart, G. Benoit, J. D. Joannopoulos, and Y. Fink, "Wavelength-scalable hollow optical fibres with large photonic bandgaps for CO_2 laser transmission," Nature **420**, 650–653 (2002).
46. F. Ozturk, A. Yildirim, M. Kanik, and M. Bayindir, "Photonic bandgap narrowing in conical hollow core Bragg fibers," Appl. Phys. Lett. **105**, 071102 (2014).
47. M. Yaman, A. Yildirim, M. Kanik, T. C. Cinkara, and M. Bayindir, "High selectivity Boolean olfaction using hollow-core wavelength-scalable Bragg fibers," Anal. Chem. **84**, 83–90 (2012).
48. A. Yildirim, F. Ozturk, and M. Bayindir, "Smelling in chemically complex environments: an optofluidic Bragg fiber array for differentiation of methanol adulterated beverages," Anal. Chem. **85**, 6384–6391 (2013).
49. H. E. Kondakci, M. Yaman, O. Koylu, A. Dana, and M. Bayindir, "All-chalcogenide glass omnidirectional photonic band gap variable infrared filters," Appl. Phys. Lett. **94**, 111110 (2009).